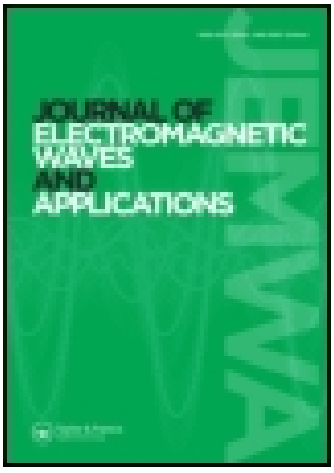

Journal of Electromagnetic Waves and Applications

Publication details, including instructions for authors and subscription information:
http://www.tandfonline.com/loi/tewa20

A traveling-wave model of electric machines with eccentricity for shaft voltage analysis

Alireza Abbasi[a] & Jalal Nazarzadeh[a]

[a] Department of Electrical Engineering, Shahed University, Tehran, Iran.

Published online: 08 Oct 2014.

To cite this article: Alireza Abbasi & Jalal Nazarzadeh (2014): A traveling-wave model of electric machines with eccentricity for shaft voltage analysis, Journal of Electromagnetic Waves and Applications

To link to this article: http://dx.doi.org/10.1080/09205071.2014.964373

Journal of Electromagnetic Waves and Applications, 2014
http://dx.doi.org/10.1080/09205071.2014.964373

Taylor & Francis
Taylor & Francis Group

A traveling-wave model of electric machines with eccentricity for shaft voltage analysis

Alireza Abbasi and Jalal Nazarzadeh*

Department of Electrical Engineering, Shahed University, Tehran, Iran

(*Received 30 June 2014; accepted 4 September 2014*)

This paper presents a discrete model for rotor shaft and stator winding of an electrical machine. Multi-conductor transmission line theory is used for modeling connecting cable, stator winding, and rotor shaft. The conductors used in a stator winding are connected similarly to a multi-conductor transmission line using electrical and magnetic coupling effects. Modal theory is applied to the wave equations of the stator winding to obtain a discrete model for electrical machines winding. The voltage distribution in the stator winding, rotor shaft, and bearings were obtained by numerical simulation under symmetrical conditions and compared with published results for time-domain method. The consequences of a static eccentricity fault on shaft voltage were determined and evaluated using a symmetrical machine.

Keywords: electrical machines; modal theory; shaft voltage; stator winding; traveling-wave model

1. Introduction

Rotary electrical machines with power electronic drives are common equipments in electrical drive systems. The existence of shaft voltage in electrical machines with sinusoidal waveforms is a well-known problem.[1] Shaft currents flow along the surface of the bearing in response to shaft voltage. The shaft current and voltage can be determined from the oil color, holes in the bearing, and shaft deformation. To avert a mechanical tension and possible failure,[2] the current density on the bearing surface should not exceed more than 1 amp/in^2.[3] A voltage source inverter with PWM control methods can produce extra bearing current in electrical machines.[4] The inverter generates common mode voltages on the stator windings and a capacitive coupling current flows on the bearings.[5] If a machine is shielded with foil and insulating layers in the air gap between the rotor and stator or with copper foil on the cover of the stator slots, the shaft current and voltage will decrease or disappear.[6] The relationship between shaft current and voltage can be affected by parasitic capacitors in the machine.[7] It is possible to decrease the critical effect of common mode currents produced by a PWM voltage source inverter.[8] Hard- and soft-switching control methods [9] and limiting switching technique in three-level inverters [10] are approaches for decreasing shaft current and voltage. The length of the cable and bearing insulation can affect the amplitude of shaft voltage and current, respectively, in electrical machines.[11,12] An imbalance in the inductance and capacitance of conductors in an electrical machine with an unsymmetrical air gap can increase shaft voltage and current.[13] Differential and common mode filters for motor–inverter systems can decrease shaft voltage amplitude in machines

*Corresponding author. Email: nazarzadeh@shahed.ac.ir

by inserting an impedance circuit between the machine and the inverter.[14,15] Inserting insulating material between the outer race of bearings and the machine frame can prevent the flow of the bearing currents by shaft voltage.[16]

[17] introduced a lumped circuit model of an electric motor to analyze electromagnetic interference (EMI) and shaft voltage. In their model, the capacitances of the stator conductor and rotor frame were obtained based on theoretical analysis and measurement results; however, the proposed model was not capable of analyzing the shaft voltage and EMI at high frequencies. Capacitance coupling between a stator winding and a rotor frame effectively produces shaft voltage. In the design stage of an electrical machine, the use of correct dimensions for the stator slot, the air gap distance between the slot gear and the stator winding, and the height of the slot gear decreases the induced voltage on the shaft and the destructive effects of current on ball bearings.[18]

Stator winding can be modeled as a three-phase transmission line using a combination of Clarke and Laplace transformations.[19] Because of the small skin depth of the magnetic core in rotary machines under high-frequency excitation, rotor frame, and stator conductors should be described using the wave propagation theory. The capacitance and inductance of the conductors and the rotor frame can be modeled using the finite element method (FEM). McLaren and Oraee [20] used a 2D FEM model to find the capacitance and inductance of the stator winding slot and overhang regions. In their study, stator conductors were shown as a multi-conductor transmission lines connected in series. Wang et al. [21] obtained an accurate estimation of conductor voltage by modeling a cable between the machine and the inverter as a transmission line and the induction machine as a lumped device. In this method, the stator winding and rotor frame are not distributed elements and thus, it cannot be used to accurately obtain the internal and shaft voltage distributions. Several studies have tried to model and simulate EMI and bearing current and loss.[22] Vivo et al. [23] introduced a multi-conductor transmission line for stator coils and the part of the rotor shaft near by a slot. In this model, the part of the rotor shaft was shown as a conductor per slot; however, the rotor shaft was used multiple times per coil in the system equations. A more efficient and accurate method should be prepared to model and simulate the EMI, bearing current, and voltage of converters and electrical machines.

The present study introduces a discrete model for electrical machines to analyze the voltage distributions in the stator winding, rotor shaft, and bearings. The stator winding and rotor shaft are modeled based on the multi-conductor transmission line theory in the modal domain. In this domain, a transmission line with n conductors is transformed into n separate single-conductor lines by n system modes. The modal transformation matrices are obtained using eigenvectors of the capacitance and inductance matrices of the system. The current and voltage distributions on the stator conductors and rotor shaft are simulated and the results are provided. The cable length, source voltage rise time, and unsymmetrical air gap that effect current and voltage distributions in electrical machines are investigated.

2. Capacitance and inductance in an electric machine

The distributed voltage in a coil depends on the characteristics of the electrical insulation and the slot geometry of an electrical machine. When an electrical machine is supplied by a switching voltage source inverter, common mode voltage with high amplitude and frequency will be produced on the stator coils. An undesired profile for distributed voltage can cause partial discharge into the insulating materials. The parasitic coupling capacitance and inductance between all parts of an electrical machine must be found to model this phenomenon. The capacitors between the stator conductors and stator frame (C_{ws}), and

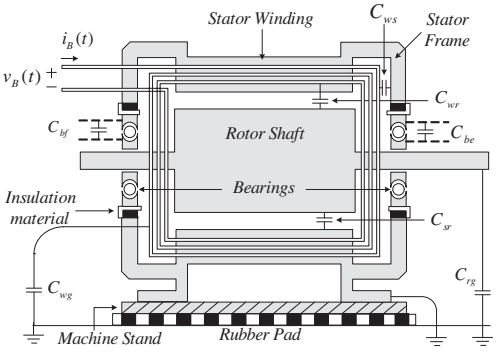

(a) Schematic of electric machine

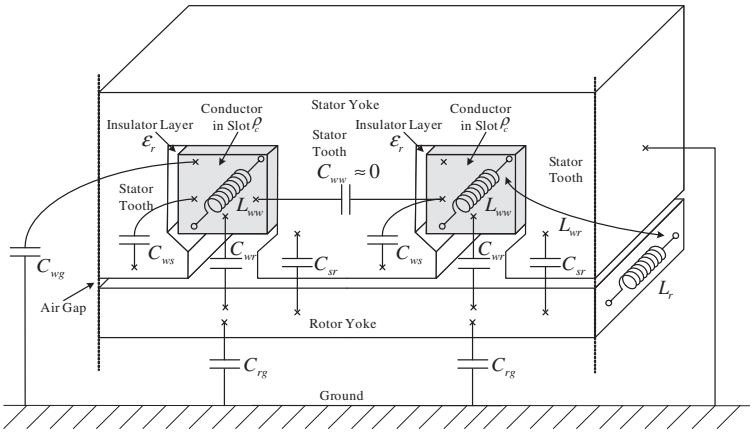

(b) Capacitance and inductance of conductor in slot

Figure 1. Structure of electric machine with inductance and parasitic capacitance.

the rotor frame (C_{wr}) are illustrated in Figure 1. These capacitors can produce significant unwanted effects at high frequencies. C_{sg}, C_{rg}, and C_{wg} are the capacitances of the stator, rotor, and conductors to the ground, respectively. These capacitors can be obtained by FEM when the detail geometry and material characteristics of the electrical machine are available. The air gap capacitor (C_{sr}) provides the electrical coupling between the stator and rotor frame. The fixed and rotating sections of some bearings may be insulated as shown for the bearing capacitors (C_{bf} and C_{be}) in Figure 1(a).

Figure 1(b) is a sectional scheme of a conductor inside a slot with assumed resistivity ρ_b and insulated by a dielectric layer with relative permittivity ϵ_r. The conductor can be bound in a slot using multiple insulators with different constant dielectrics and thicknesses. Details of the structure of conductors in a slot are shown in Figure A1(a). The dielectrics are given in linear, isotropic, and homogenate forms. The computation error is less than 1% when dielectric loss from the insulation is ignored.[24]

Conductors in the slot, stator, and rotor frames can experience high-frequency currents. Self-inductance and mutual inductance of all components in an electrical machine are shown in Figure 1(b). L_{ww} and L_r are the self-inductances of the conductor and rotor frames, respectively. L_{wr} is the mutual inductance between the stator conductor and rotor frame. The capacitance ($\mathbf{C_k}$) and inductance ($\mathbf{L_k}$) matrices in different parts of an electrical machine

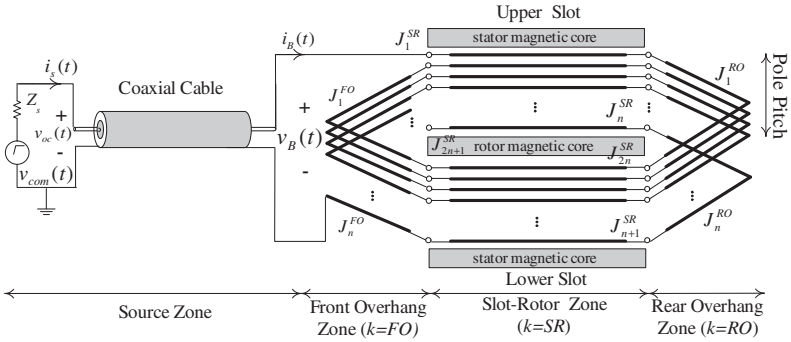

Figure 2. Stator windings connected to common mode voltage source.

can be obtained using the structure of Figure 1(b). These matrices are symmetrical and can be applied to find the wave propagation model of the electrical machine at high frequencies.

3. Transmission line model of stator windings

Electrical and magnetic coupling fields impress current and voltage on all conductors in the same zone. Figure 2 is a simple model of stator winding with n coils in different zones. These coils are formed by four conductors in the front overhang (FO), slot-rotor (SR), and rear overhang (RO) zones. They can be divided into four segments in the connection series.

The SR zone is the magnetic core of an electric machine. In this zone, the conductors are located inside the stator slots. The FO and RO zones are outside of the slots in the overhang. Figure 2 shows J_n^{FO}, J_n^{SR}, and J_n^{RO} in the nth conductor of the stator coil in the FO, SR, and RO zones, respectively. The conductors in one zone can be coupled; therefore, a portion of the winding in that zone can be assumed to be a multi-conductor transmission line with specific boundary conditions. Conductors in different zones (with different k indices) cannot be directly coupled. Figure 3 shows the winding of the electrical machine from Figure 2 showing the multi-conductor transmission lines in the three zones. The inductance and capacitance matrices of conductors in one zone can be found using FEM.

4. Traveling-wave model of multi-conductor transmission line

A traveling-wave model of a multi-conductor transmission line with the three zones was used to examine the high-frequency behavior of stator winding in an electrical machine. Figure 3 shows 3 p_k-conductor transmission lines in FO, SR, and RO zones. The number of conductors (p_k) in the FO, SR, and RO zones are n, $2n+1$, and n, respectively. The conductors are not coupled between the different zones. Figure 4 shows the multi-conductor transmission lines for FO, SR, and RO zones.

Traveling wave equations in the kth zone ($k =$ FO, SR, and RO) can be written as:

$$\begin{aligned} \frac{\partial \boldsymbol{v}_k(x,t)}{\partial x} &= -\mathbf{L}_k \frac{\partial \boldsymbol{i}_k(x,t)}{\partial t} \\ \frac{\partial \boldsymbol{i}_k(x,t)}{\partial x} &= -\mathbf{C}_k \frac{\partial \boldsymbol{v}_k(x,t)}{\partial t} \end{aligned} \qquad k = FO,\ SR \text{ and } RO \tag{1}$$

in which $\mathbf{C}_k$ and $\mathbf{L}_k$ are the capacitance and inductance matrices of the p_k-conductor in per unit length, respectively. Also, $\boldsymbol{i}_k(x,t)$ and $\boldsymbol{v}_k(x,t)$ are current and voltage vectors of the

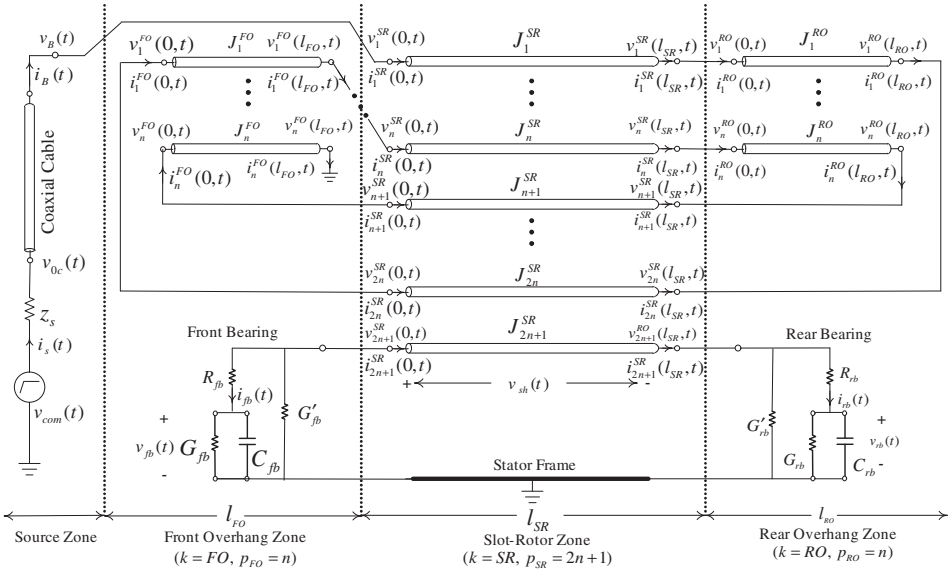

Figure 3. Transmission line model of stator winding.

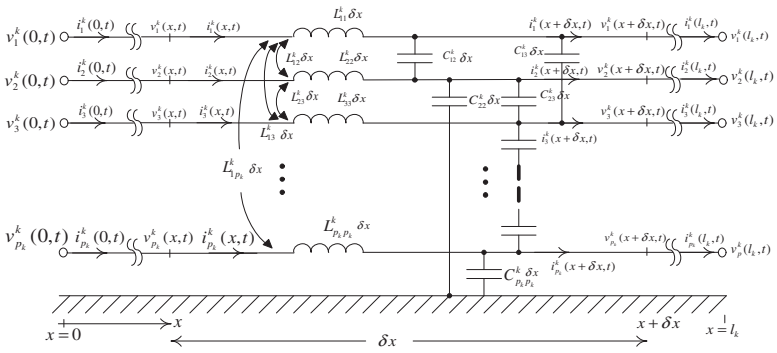

Figure 4. p_k-conductor loss less transmission line in the kth zone.

transmission line in the kth zone at t and x. These vectors are given as:

$$\begin{aligned} \boldsymbol{v}_k(x,t) &= \begin{pmatrix} v_1^k(x,t) & v_2^k(x,t) & \cdots & v_{p_k}^k(x,t) \end{pmatrix}^T \\ \boldsymbol{i}_k(x,t) &= \begin{pmatrix} i_1^k(x,t) & i_2^k(x,t) & \cdots & i_{p_k}^k(x,t) \end{pmatrix}^T \end{aligned} \tag{2}$$

Superscript T means transpose of a matrix or a vector. $\mathbf{L}_{FO}$, $\mathbf{L}_{RO}$, $\mathbf{C}_{FO}$, and $\mathbf{C}_{RO}$ are $n \times n$ symmetrical matrices in per unit. Theses matrices illustrate the distributed inductance and shunt capacitance of n-conductor transmission line in FO and RO zones. $\mathbf{L}_{SR}$ and $\mathbf{C}_{SR}$ are $(2n+1)\times(2n+1)$ symmetrical matrices that present distributed inductance and capacitance of the $(2n+1)$-conductor transmission line in per-unit. These matrices can be suggested as:

$$\mathbf{L}_{SR} = \left[\begin{array}{c:c|c} \mathbf{L}_{us} & \mathbf{L}_{uls} & \\ \hdashline \mathbf{L}_{uls}^T & \mathbf{L}_{ls} & \mathbf{L}_m \\ \hline \multicolumn{2}{c|}{\mathbf{L}_m^T} & L_r \end{array}\right] \tag{3}$$

$$\mathbf{C}_{SR} = \left[\begin{array}{c:c|c} \mathbf{C}_{us} & \mathbf{0}_n & \\ \hdashline \mathbf{0}_n & \mathbf{C}_{ls} & \mathbf{C}_m \\ \hline \multicolumn{2}{c|}{\mathbf{C}_m^T} & c_r \end{array}\right] \tag{4}$$

where $\mathbf{L}_{us}$, $\mathbf{L}_{ls}$, and $\mathbf{L}_{usl}$ are $n \times n$ matrices of the upper, lower, and slot mutual inductances, respectively. $\mathbf{C}_{us}$ and $\mathbf{C}_{ls}$ are $n \times n$ upper and lower capacitance matrices of n-conductor in upper and lower slots. $\mathbf{L}_m$ and $\mathbf{C}_m$ are $2n \times 1$ column vectors for illustrating coupling inductance and capacitance of the rotor and 2n-conductors and L_r and c_r are two scalar values of the rotor self-inductance and capacitance. $\mathbf{0}_n$ presents a $n \times n$ zero diagonal matrix. The traveling-wave equations in (1) are transferred into frequency domain as:

$$\begin{aligned} \frac{d^2}{dx^2}\boldsymbol{V}_k(x,s) &= s^2\boldsymbol{\Gamma}_k^2\boldsymbol{V}_k(x,s) \\ \frac{d^2}{dx^2}\boldsymbol{I}_k(x,s) &= s^2(\boldsymbol{\Gamma}_k^2)^T\boldsymbol{I}_k(x,s) \end{aligned} \tag{5}$$

where $\boldsymbol{V}_k(x,s)$ and $\boldsymbol{I}_k(x,s)$ are the Laplace transforms of $\boldsymbol{v}_k(x,t)$ and $\boldsymbol{i}_k(x,t)$, respectively. $\boldsymbol{\Gamma}_k$ is the propagation constant matrix of the multi-conductor transmission line. Using (1) and (5), we can write:

$$\boldsymbol{\Gamma}_k^2 = \mathbf{L}_k\mathbf{C}_k \tag{6}$$

A multi-conductor transmission line can be analyzed with a modal technique. Velocity and impedance of each mode are determined using propagation constant matrix ($\boldsymbol{\Gamma}$) in diagonal form ($\boldsymbol{\Lambda}_k^2$) as:

$$\begin{aligned} \boldsymbol{\Lambda}_k^2 &= \mathbf{T}_k^{-1}\boldsymbol{\Gamma}_k^2\mathbf{T}_k \\ &= \mathbf{T}_k^T(\boldsymbol{\Gamma}_k^2)^T(\mathbf{T}_k^{-1})^T \end{aligned} \tag{7}$$

where $\mathbf{T}_k$ is a similarity transformation and is obtained from eigenvectors of $\boldsymbol{\Gamma}_k^2$. The pth diagonal element of $\boldsymbol{\Lambda}_k^2$ is given by ${\lambda_p^k}^2$. The diagonal form of the traveling wave equations are obtained by applying (5)–(7) as:

$$\begin{aligned} \frac{d^2}{dx^2}\boldsymbol{E}_k(x,s) &= s^2\boldsymbol{\Lambda}_k^2\boldsymbol{E}_k(x,s) \\ \frac{d^2}{dx^2}\boldsymbol{J}_k(x,s) &= s^2\boldsymbol{\Lambda}_k^2\boldsymbol{J}_k(x,s) \end{aligned} \tag{8}$$

where $\boldsymbol{E}_k(x,s)$ and $\boldsymbol{J}_k(x,s)$ are vectors of voltage and current of the multi-conductor transmission line in modal quantities. These vectors are determined by:

$$\begin{aligned}\boldsymbol{E}_k(x,s) &= \mathbf{T}_k^{-1}\boldsymbol{V}_k(x,s)\\ \boldsymbol{J}_k(x,s) &= \mathbf{T}_k^{T}\boldsymbol{I}_k(x,s)\end{aligned} \tag{9}$$

Using (1) and (9), we can write:

$$\begin{aligned}\mathbf{L}'_k &= \mathbf{T}_k^{-1}\mathbf{L}_k(\mathbf{T}_k^{-1})^T\\ \mathbf{C}'_k &= \mathbf{T}_k^{T}\mathbf{C}_k\mathbf{T}_k\end{aligned} \tag{10}$$

where $\mathbf{L}'_k$ and $\mathbf{C}'_k$ are $p_k \times p_k$ diagonal inductance and capacitance matrices in modal quantities. The pth diagonal element of $\mathbf{L}'_k$ and $\mathbf{C}'_k$ are L'^k_p and C'^k_p, respectively. The pth relation of (8) is written as:

$$\begin{aligned}\frac{d^2}{dx^2}e_p^k(x,s) &= s^2{\lambda_p^k}^2 e_p^k(x,s)\\ \frac{d^2}{dx^2}j_p^k(x,s) &= s^2{\lambda_p^k}^2 j_p^k(x,s)\end{aligned} \qquad \begin{aligned}&p = 1,\cdots,p_k\\ &k = \text{FO, SR and RO}\end{aligned} \tag{11}$$

where $e_p^k(x,s)$ and $j_p^k(x,s)$ are the voltage and current of the pth conductor in modal quantities in the kth zone. These relations present lossless single-phase transmission line without any electrical and magnetic coupling with other conductors. The voltage and current of the conductor in modal quantities are introduced using traveling wave equations as [25]:

$$\begin{aligned}e_p^k(x,t) + Z_p^k j_p^k(x,t) &= 2e_p^{k+}\left(t - \frac{x}{v_p^k}\right)\\ e_p^k(x,t) - Z_p^k j_p^k(x,t) &= 2e_p^{k-}\left(t + \frac{x}{v_p^k}\right)\end{aligned} \tag{12}$$

in which

$$Z_p^k = \sqrt{\frac{L'^k_p}{C'^k_p}} \quad v_p^k = \frac{1}{\sqrt{L'^k_p C'^k_p}} \tag{13}$$

Z_p^k and v_p^k are the characteristic impedance and wave velocity of the pth single-conductor transmission line at the kth zone. $e_p^{k+}(t - \frac{x}{v_p^k})$ and $e_p^{k-}(t + \frac{x}{v_p^k})$ are the pth forward and backward traveling waves. Voltage of the input terminal ($e_p^k(0,t)$) is determined using the first relation in (12) as:

$$e_p^k(0,t) + Z_p^k j_p^k(0,t) = 2e_p^{k+}(t) \tag{14}$$

The forward traveling wave ($e_p^{k+}(t)$) receives $x = l_k$ (output terminal) after $\tau_p^k = \frac{l_k}{v_p^k}$. So, the voltage of the output terminal $e_p^k(l_k,t)$ is determined from:

$$e_p^k(l_k,t) + Z_p^k j_p^k(l_k,t) = 2e_p^{k+}\left(t - \tau_p^k\right) \tag{15}$$

By combining (14) and (15), we have:

$$e_p^k(0,t-\tau_p^k) + Z_p^k j_p^k(0,t-\tau_p^k) = e_p^k(l_k,t) + Z_p^k j_p^k(l_k,t) \tag{16}$$

The similar result is found using the second relation in (12).

$$e_p^k(l_k,t-\tau_p^k) - Z_p^k j_p^k(l_k,t-\tau_p^k) = e_p^k(0,t) - Z_p^k j_p^k(0,t) \tag{17}$$

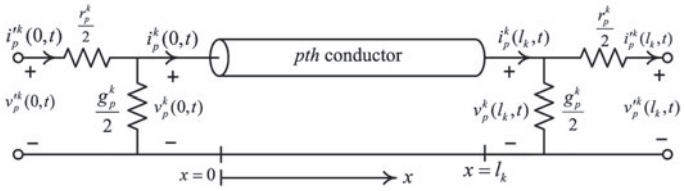

Figure 5. Schematic of the pth conductor in the kth region.

The relations (16) and (17) present a discrete model of single-conductor transmission line in modal quantities ($p = 1, \ldots, p_k$ and k =FO, SR, and RO). These relations can be expressed in vector form as:

$$\begin{aligned} \boldsymbol{e}_k(0, t-\tau_k) + \mathbf{Z}_k \boldsymbol{j}_k(0, t-\tau_k) &= \boldsymbol{e}_k(l_k, t) + \mathbf{Z}_k \boldsymbol{j}_k(l_k, t) \\ \boldsymbol{e}_k(l_k, t-\tau_k) - \mathbf{Z}_k \boldsymbol{j}_k(l_k, t-\tau_k) &= \boldsymbol{e}_k(0, t) - \mathbf{Z}_k \boldsymbol{j}_k(0, t) \end{aligned} \tag{18}$$

in which

$$\begin{aligned} \boldsymbol{e}_k(x,t) &= \begin{pmatrix} e_1^k(x,t) & e_2^k(x,t) & \cdots & e_{p_k}^k(x,t) \end{pmatrix}^T \\ \boldsymbol{j}_k(x,t) &= \begin{pmatrix} j_1^k(x,t) & j_2^k(x,t) & \cdots & j_{p_k}^k(x,t) \end{pmatrix}^T \end{aligned} \tag{19}$$

$\mathbf{Z}_k$ is a $p_k \times p_k$ diagonal impedance matrix, given as:

$$\mathbf{Z}_k = diag \begin{pmatrix} Z_1^k & Z_2^k & \cdots & Z_{p_k}^k \end{pmatrix} \tag{20}$$

The relation between voltage and current vectors in real domain are determined using combining (9) and (18) as:

$$\begin{aligned} \boldsymbol{v}_k(0, t-\tau_k) + \mathbf{Z}'_k \boldsymbol{i}_k(0, t-\tau_k) &= \boldsymbol{v}_k(l_k, t) + \mathbf{Z}'_k \boldsymbol{i}_k(l_k, t) \\ \boldsymbol{v}_k(l_k, t-\tau_k) - \mathbf{Z}'_k \boldsymbol{i}_k(l_k, t-\tau_k) &= \boldsymbol{v}_k(0, t) - \mathbf{Z}'_k \boldsymbol{i}_k(0, t) \end{aligned} \tag{21}$$

where

$$\mathbf{Z}'_k = \mathbf{T}_k \mathbf{Z}_k \mathbf{T}_k^{-1} \tag{22}$$

The series resistance and transversal conductance in the discrete model are ignored. A conventional method for including series resistance and transversal conductance is shown in Figure 5. A total series and shunt resistances of the pth conductor (r_p^k and g_p^k) are divided into two equal parts and inserted in the terminals. The input ($\boldsymbol{i}'_k(0,t)$) and output ($\boldsymbol{i}'_k(l_k,t)$) vector currents are determined as:

$$\begin{aligned} \boldsymbol{i}'_k(0,t) &= \boldsymbol{i}_k(0,t) + \tfrac{1}{2}\mathbf{G}_k \boldsymbol{v}_k(0,t) \\ \boldsymbol{i}'_k(l_k,t) &= \boldsymbol{i}_k(l_k,t) - \tfrac{1}{2}\mathbf{G}_k \boldsymbol{v}_k(l_k,t) \end{aligned} \tag{23}$$

in which $\boldsymbol{i}'_k(x,t)$ and $\mathbf{G}_k$ are $p_k \times 1$ and $p_k \times p_k$ matrices as:

$$\boldsymbol{i}'_k(x,t) = \left(i'^k_1(x,t) i'^k_2(x,t) \cdots i'^k_{p_k}(x,t) \right)^T \tag{24}$$

$$\mathbf{G}_k = diag \begin{pmatrix} g_1^k & g_2^k \cdots g_{p_k}^k \end{pmatrix} \tag{25}$$

Similarly, the input ($\boldsymbol{v}'_k(0,t)$) and output ($\boldsymbol{v}'_k(l_k,t)$) voltages are obtained as:

$$\begin{aligned} \boldsymbol{v}'_k(0,t) &= \boldsymbol{v}_k(0,t) + \frac{1}{2}\mathbf{R}_k \boldsymbol{i}'_k(0,t) \\ \boldsymbol{v}'_k(l_k,t) &= \boldsymbol{v}_k(l_k,t) - \frac{1}{2}\mathbf{R}_k \boldsymbol{i}'_k(l_k,t) \end{aligned} \tag{26}$$

in which $\boldsymbol{v}'_k(x,t)$ and $\mathbf{R}_k$ are $p_k \times 1$ and $p_k \times p_k$ matrices, given as:

$$\boldsymbol{v}'_k(x,t) = \begin{pmatrix} v'^k_1(x,t) & v'^k_2(x,t) & \cdots & v'^k_{p_k}(x,t) \end{pmatrix}^T \tag{27}$$

$$\mathbf{R}_k = diag\begin{pmatrix} r^k_1 & r^k_2 & \cdots & r^k_{p_k} \end{pmatrix} \tag{28}$$

If vectors of $\boldsymbol{i}_k(0,t), \boldsymbol{i}_k(l_k,t), \boldsymbol{v}_k(0,t)$, and $\boldsymbol{v}_k(l_k,t)$ are solved from (23) and (26) and results are substituted into (21), discrete relations for terminal voltage and current in kth zone will be found as:

$$\begin{aligned} \hat{\boldsymbol{\sigma}}_k \boldsymbol{v}'_k(0,t-\tau_k) + \hat{\mathbf{Z}}_k \boldsymbol{i}'_k(0,t-\tau_k) &= \hat{\boldsymbol{\sigma}}'_k \boldsymbol{v}'_k(l_k,t) + \hat{\mathbf{Z}}'_k \boldsymbol{i}'_k(l_k,t) \\ \hat{\boldsymbol{\sigma}}_k \boldsymbol{v}'_k(l_k,t-\tau_k) - \hat{\mathbf{Z}}_k \boldsymbol{i}'_k(l_k,t-\tau_k) &= \hat{\boldsymbol{\sigma}}'_k \boldsymbol{v}'_k(0,t) - \hat{\mathbf{Z}}'_k \boldsymbol{i}'_k(0,t) \end{aligned} \tag{29}$$

in which

$$\begin{aligned} \hat{\boldsymbol{\sigma}}_k &= \mathbf{I} - \frac{1}{2}\mathbf{Z}'_k\mathbf{G}_k \\ \hat{\boldsymbol{\sigma}}'_k &= \mathbf{I} + \frac{1}{2}\mathbf{Z}'_k\mathbf{G}_k \\ \hat{\mathbf{Z}}_k &= \mathbf{Z}'_k - \frac{1}{2}\mathbf{R}_k + \frac{1}{4}\mathbf{Z}'_k\mathbf{G}_k\mathbf{R}_k \\ \hat{\mathbf{Z}}'_k &= \mathbf{Z}'_k + \frac{1}{2}\mathbf{R}_k + \frac{1}{4}\mathbf{Z}'_k\mathbf{G}_k\mathbf{R}_k \end{aligned} \tag{30}$$

The discrete relations in (29) are extended to all conductors in the three zones ($k =$ FO, SR, and RO) and used to determine terminal currents and voltages of conductors based on the suitable boundary conditions that are presented in the following section.

5. Boundary conditions

The input and output terminals of a conductor in Figure 3 are directly connected to other conductors in different zones. Boundary conditions of terminal voltages can be described as:

$$\begin{aligned} v'^{SR}_1(0,t) &= v_B(t) \quad v'^{SR}_{p+1}(0,t) = v'^{FO}_p(l_{FO},t) \\ i'^{SR}_1(0,t) &= i_B(t) \quad i'^{SR}_{p+1}(0,t) = i'^{FO}_p(l_{FO},t) \end{aligned} \qquad p = 1,\cdots,n-1 \tag{31}$$

In addition, the end of the nth front overhang conductor is connected to ground ($v'^{FO}_n(l_{FO},t) = 0$). Other boundary conditions are:

$$\begin{aligned} v'^{SR}_p(l_{SR},t) &= v'^{RO}_p(0,t) & i'^{SR}_p(l_{SR},t) &= i'^{RO}_p(0,t) \\ v'^{SR}_{2n+1-p}(l_{SR},t) &= v'^{RO}_p(l_{RO},t) & i'^{SR}_{2n+1-p}(l_{SR},t) &= -i'^{RO}_p(l_{RO},t) \qquad p = 1,\ldots,n \\ v'^{SR}_{2n+1-p}(0,t) &= v'^{FO}_p(0,t) & i'^{SR}_{2n+1-p}(0,t) &= -i'^{FO}_p(0,t) \end{aligned} \tag{32}$$

In some cases such as Figure 3, a linear lumped capacitor may be connected to a transmission line at input or output terminals. The front and rear bearings with lumped resistor and capacitor are connected to the input and output terminals of the rotor frame (the $(2n+1)$th conductor in SR zone). The first-order differential equation for the front bearing voltage ($v_{fb}(t)$) is:

$$R_{fb}C_{fb}\frac{d}{dt}v_{fb}(t) + \left(G_{fb}R_{fb} + 1\right)v_{fb}(t) = v'^{FO}_{2n+1}(0,t) \tag{33}$$

where R_{fb}, G_{fb}, and C_{fb} are the series resistance, paralleled conductance, and capacitance of the front bearing, respectively. By integrating (33) between $t-\tau$ to t and applying

trapezoidal integration lemma, a discrete relation between input and capacitor voltages can be determined as:

$$\left(G_{fb}R_{fb}+\frac{2}{\tau}R_{fb}C_{fb}+1\right)v_{fb}(t)+\left(G_{fb}R_{fb}-\frac{2}{\tau}R_{fb}C_{fb}+1\right)v_{fb}(t-\tau)$$
$$=v'^{SR}_{2n+1}(0,t)+v'^{SR}_{2n+1}(0,t-\tau) \tag{34}$$

Similarly, discrete relation for the rear bearing voltage (v_{rb}) is:

$$\left(G_{rb}R_{rb}+\frac{2}{\tau}R_{rb}C_{rb}+1\right)v_{rb}(t)+\left(G_{rb}R_{rb}-\frac{2}{\tau}R_{rb}C_{rb}+1\right)v_{rb}(t-\tau)$$
$$=v'^{SR}_{2n+1}(l_{SR},t)+v'^{SR}_{2n+1}(l_{SR},t-\tau) \tag{35}$$

where R_{rb}, G_{rb}, and C_{rb} are the series resistance, paralleled conductance, and capacitance of the rear bearing, respectively. The boundary conditions of rotor shaft in front and rear bearings are:

$$\frac{R_{fb}+R'_{fb}}{R'_{fb}}v'^{SR}_{2n+1}(0,t)+R_{fb}i'^{SR}_{2n+1}(0,t)=v_{fb}(t)$$
$$\frac{R_{rb}+R'_{rb}}{R'_{rb}}v'^{SR}_{2n+1}(l_{SR},t)-R_{rb}i'^{SR}_{2n+1}(l_{SR},t)=v_{rb}(t) \tag{36}$$

6. Numerical results

The structure of an induction machine was used to develop the discrete model. The structural detail and parameters of the machine are shown in the appendix. The voltage distribution in the stator conductors was analyzed using the time-domain equivalent circuit method suggested by [26]. The capacitance and inductance matrices of the system can be determined in (1) using the machine parameters provided in the appendix. The distributed voltage of the winding can be obtained from (29), (34), and (35) with boundary conditions in (31), (32), and (36) at $n = 10$. Figure 6(a) shows the input voltage of the stator winding ($v_B(t)$) in the propagation model of the proposed machine at different cable lengths ($l_c = 5$, 10, and 20 m). The rise time (t_s) of the input voltage to the stator winding ($v_{com}(t)$) is $t_s = 400$ ns. It is evident from the results that cable length influences the voltage wave distribution. Increasing the cable length up to a specific amount produces the impedance mismatch in the motor terminal and increases the output voltage of the cable to above maximum voltage. When the length of the cable increases, the frequency of coil voltage decreases in response to the change in transition times and oscillating waves.

The influence of rise time t_s on the input voltage of the stator winding ($v_B(t)$) for surge rise times of 50, 200, and 600 ns at $l_c = 10$ m is shown in Figure 6(b). It is evident that decreasing the rise time t_s increased the magnitude and rate of winding voltage. Table (A1) provides a comparison of the proposed method and the results of other studies using the time-domain technique [26] and the maximum input voltages for different t_s and l_c are listed. Figure 7 shows voltage propagation along the stator winding at the end of a turn at $l_c = 10$ m and different times for the source voltage.

Figure 8 shows the shaft voltage $(v)sh(t)$ of the electrical machine. The shaft voltage was determined as the difference between the front and rear bearing voltages. The bearing parameters of the machine are provided in the appendix. These results illustrate that the percentage of maximum overvoltage is 5.93% for a 400 ns rise time at the common voltage of the stator winding and a cable length of 10 m.

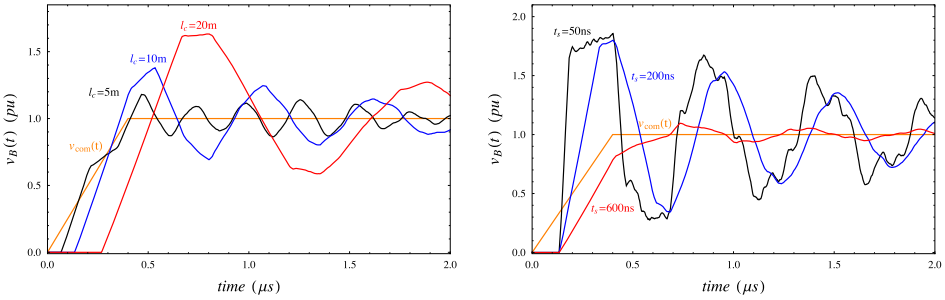

(a) Different l_c with $t_s = 400ns$ (b) Different t_s with $l_c = 10m$

Figure 6. Input voltage of the winding with different l_c and t_s.

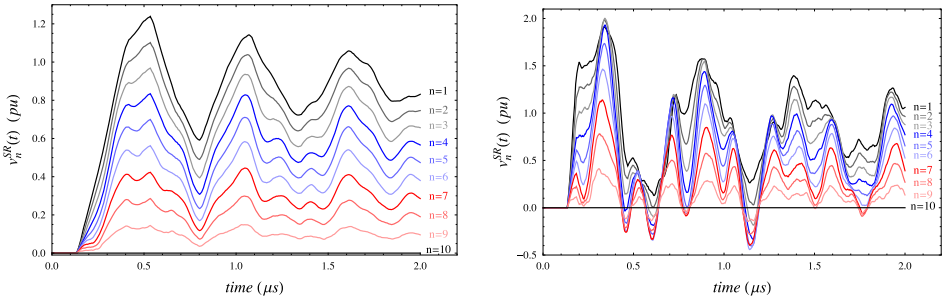

(a) $t_s = 400\ ns$ (b) $t_s = 50\ ns$

Figure 7. Voltage distribution in end of coils with $l_c = 10$ m and different t_s.

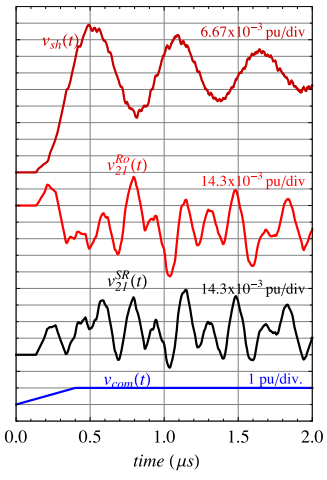

Figure 8. Shaft and bearing voltages with $l_c = 10$ m and $t_s = 400$ ns.

In part of the PWM switching voltage, the common voltage is similar to that shown in Figure 9(a). In this case, the rate of the common voltage has different sign in times; therefore, overvoltages of the stator coils appear repeatedly at 5.36%.

The structure of the machine with air gap eccentricity shown in Figure A1(b) is presented in the appendix. The air gap eccentricity is the displacement of the rotor center and d is

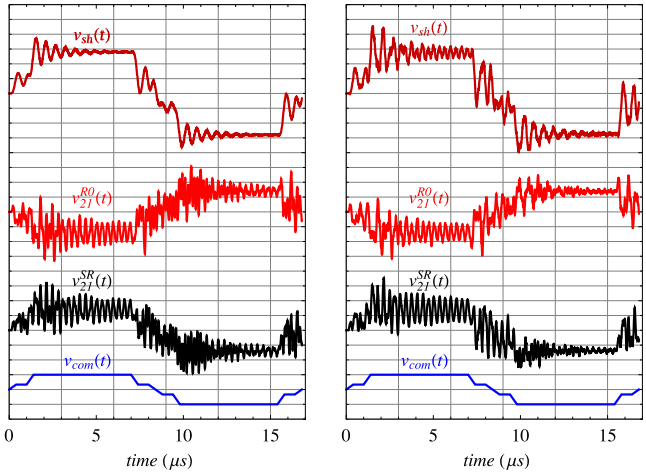

(a) Symmetric air gap (b) Asymmetric air gap

Figure 9. Shaft voltages with a switching pattern, $l_c = 10\,\text{m}$ and $t_s = 400\,\text{ns}$; scale: v_{com}: 1 pu/div., v_{21}^{SR}, v_{21}^{RO} and v_{sh}: 14.29×10^{-3} pu/div.

the eccentricity index for the air gap. The appendix evaluates the effect of the index on the capacitance and inductance matrices and shows that the capacitance matrix experiences no noticeable effect from the air gap eccentricity. The shaft voltage of the proposed machine can be obtained by replacing the inductance matrix of the system with 50% air gap eccentricity ($d = 1$ mm). Figure 9(b) shows the voltage as $d = 1$ mm when stator winding was supplied with switching source voltage. In this case, the maximum overvoltage increased to 6.46%. This result shows that the amplitude of the shaft voltage can be used to monitor the air gap eccentricity of an electrical machine.

7. Conclusion

The present study introduces voltage propagation along the stator winding and the rotor shaft. The wave propagation method was applied to multi-conductor transmission lines and the voltages and currents of the stator winding inside the slot and the overhang in the discrete system were determined using the modal theory. The voltage distribution on the machine shaft and conductors and effective factors such as the cable length and rise time of the source voltage were studied. The results of numerical studies show that this method can adequately analyze a complex problem such as shaft voltage in an electrical machine.

References

[1] Alger P, Samson H. Shaft currents in electric machines. Trans. AIEE. 1924;XLIII:235–245.
[2] Rezig A, Ndiye A, Djerdir A, Mekideche MR. Experimental investigation of vibration monitoring technique for online detection of bearing fault in induction motors. J. Electromagn. Waves Appl. 2013;27:496–506.
[3] Costello MJ. Shaft voltage and rotating machinery. IEEE Trans. Indus. Appl. 1993;IA-29: 419–426.
[4] Erdman J, Kerkman RJ, Schlegel D, Skibinski G. Effect of PWM inverters on AC motor bearing currents and shaft voltage. IEEE Trans. Indus. Appl. 1996;32:250–259.

[5] Chen S, Lipo TA, Fitzgerald D. Source of induction motor bearing currents caused by PWM inverters. IEEE Trans. Energy Conver. 1996;11:25–32.
[6] Busse D, Erdman J, Kerkman RJ, Schlegel D, Skibinski G. An evaluation of the electrostatic shielded induction motor: a solution for rotor shaft voltage build up and bearing current. In: Conference IEEE-IAS; 1996 Oct 6–10; San Diego, CA; 1996. p. 610–617.
[7] Chen S, Lipo TA, Fitzgerald D. Modeling of motor bearing currents in PWM inverter drives. In: Conference IEEE-IAS; 1995 Oct 08–12; Orlando, FL; 1995. p. 388–393.
[8] Julian AL, Lipo TA, Oriti G. Elimination of common mode voltage in three-phase sinusoidal power converters. In: Conference IEEE PESC96 1996 Jun 23, 27 ; Baveno; 1996. p. 1968–1972.
[9] Chen S, Lipo TA. Bearing currents and shaft voltages of an induction motor under hard- and soft-switching inverter excitation. IEEE Trans. Indus. Appl. 1998;35:1042–1048.
[10] Zhang H, Jouanne AEV, Dai S, Wallace AK, Wang F. Multilevel inverter modulation schemes to eliminate common-mode voltage. IEEE Trans. Indus. Appl. 2000;36:1645–1652.
[11] Muetze A, Binder AS. Calculation of influence of insulated bearings and insulated inner bearing seats on circulating bearing currents in machines of inverter-based drive system. IEEE Trans. Indus. Appl. 2006;42:965–972.
[12] Muetze A, Binder A. Calculation of motor capacitances for prediction of discharge bearing currents in machines of inverter-based drive systems. In: Proceedings of 5th IEEE International Electric Machines and Drives Conference (IEMDC); 2005 May 15; San Antonio, TX; 2005. p. 264–270.
[13] Babaei M, Faiz J, Ebrahimi BM, Amini S, Nazarzadeh J. A detailed analytical model of a salient-pole synchronous generator under dynamic eccentricity fault. IEEE Trans. Magn. 2011;47: 764–771.
[14] Muetze A, Binder A. Application of charge dissipation to mitigate electric discharge bearing currents. IEEE Trans. Indus. Appl. 2008;44:135–142.
[15] Naik R, Nondahl TA, Melfi MJ, Schiferl R, Wang JS. Circuit model for shaft voltage prediction in induction motors fed by PWM-based AC drive. IEEE Trans. Indus. Appl. 2003;39:1294–1299.
[16] Shami UT, Akagi H. Identification and discussion of the origin of a shaft end-to-end voltage in an inverter-driven motor. IEEE Trans. Indus. Appl. 2010;25:1615–1625.
[17] Zare F. Practical approach to model electric motors for electromagnetic interference and shaft voltage analysis. IET Elect. Power Appl. 2010;4:727–738.
[18] Adabi J, Zare F, Ghosh A, Lorenz RD. Calculations of capacities couplings in induction generators to analyse shaft voltage. IET Power Elec. 2010;3:379–390.
[19] Clerici D, Torre FD, Morando AP. A Form-Wound induction machine model for the study of three-phase surge propagation. IEEE Trans. Energy Conver. 2010;25:199–206.
[20] McLaren PG, Oraee H. Multi conductor transmission-line model for the line-end coil of large ac machines. IEE Proc. B (Elec. Power Appl.). 1985;132:149–155.
[21] Wang L, Ho CNM, Canales F, Jatskevich J. High-frequency modeling of the long-cable-fed induction motor drive system using TLM approach for predicting over voltage transients. IEEE Trans. Power Elec. 2010;25:2653–2664.
[22] Mütze A. Thousands of hits: on inverter-induced bearing currents, related work, and the literature. Elektrotechnik und Informationstechnik. 2011;128:382–388.
[23] Vivo BD, Tucci V, Petrarca C. Simulation of the bearing voltage in an inverter-fed induction motor by a full three phase multi conductor transmission line model. Prog. Electromagn. Res. B. 2013;46:233–250.
[24] Wedepohl LM, Nguyen HV, Irwin GD. Frequency dependent transformation matrices for untransposed transmission lines using Newton-Raphson method. IEEE Trans. Power Syst. 1996;11:1538–1546.
[25] Watson N, Arrillaga J. Power systems electromagnetic transients simulation. London: The Institution of Engineering and Technology (IET); 2007. pp. 123–156.
[26] Petrarca C, Maffucci A, Tucci V, Vitelli M. Analysis of the voltage distribution in a motor stator winding subjected to steep-fronted surge voltages by means of a multi conductor lossy transmission line model. IEEE Trans. Energy Conver. 2004;19:7–17.

Appendix 1

To apply the theory of multi-conductor transmission lines to stator winding, it is necessary to calculate the capacitance and inductance matrices and stator winding conductivity. Analytical methods can be used to calculate these parameters. Ten conductors are placed in each slot and the stator conductors are assumed to be conductors with a specific resistance (ρ_b). These conductors are insulated with dielectric materials with relative permeability (ϵ_{r1}) and thickness (δ_1). The cover binding of the conductors has an insulator with relative permeability ϵ_{r2} and thickness ϵ_{r2} . The conductors inside the slot are insulated with a dielectric with relative permeability (ϵ_{r3}) and thickness (δ_3). Figure A1(a) shows the structure of the conductors in a slot. The stator winding is connected to the voltage source by a cable with the parameters provided in Table A2. Tables A3 and A4 list the parameters of the proposed machine and bearings. This induction machine has 36 slots and 10 coils per slot. Figure A1(b) shows the rotor and stator structures of the machine with the rotor center at displacement d. In the symmetrical condition, the center displacement is $d = 0$.

A.1. Capacitance matrix of conductors

The (r, s)th element of the capacitance matrix in kth zone is:

$$c_{r,s}^{k} = \left.\frac{q_r^k(x,t)}{v_s^k(x,t)}\right|_{\substack{v_1^k(x,t)=\cdots=v_{r_k}^k(x,t)=0 \\ v_s^k(x,t)\neq 0}} \qquad \begin{array}{l} r, s = 1, \cdots, p_k \\ k = FO,\ SR \text{ and } RO \end{array} \tag{A1}$$

in which $q_r^k(x, t)$ is the charge of the rth conductor in the kth zone. The limited factor method is used to calculate the capacitance matrix in (4). The sth conductor of the coil in the kth zone is activated using 1 per unit voltage ($v_s^k(x, t) = 1\ pu$); the other conductor voltages in this zone are adjusted to zero voltage. FEM can determine the electrical field for the conductors in the kth zone. Figure A2(a) shows the electrical field of the proposed machine under symmetrical conditions ($d = 0$). The capacitance matrices of the front and rear overhangs are the same ($\mathbf{C}_{FO} = \mathbf{C}_{RO}$) in the symmetrical condition. Using (A1), the capacitance matrices for the overhang and slot in nF can be determined as:

$$\mathbf{C}_{FO} = \begin{bmatrix} 0.541 & -0.5362 & -0.004 & -0.0006 & -0.0001 & 0. & 0. & 0. & 0. & 0. \\ -0.5362 & 1.0741 & -0.5339 & -0.0034 & -0.0005 & -0.0001 & 0. & 0. & 0. & 0. \\ -0.004 & -0.5339 & 1.0755 & -0.5337 & -0.0033 & -0.0006 & -0.0001 & 0. & 0. & 0. \\ -0.0006 & -0.0034 & -0.5337 & 1.075 & -0.5333 & -0.0034 & -0.0006 & -0.0001 & 0. & 0. \\ -0.0001 & -0.0005 & -0.0033 & -0.5333 & 1.0745 & -0.5332 & -0.0034 & -0.0006 & -0.0001 & 0. \\ 0. & -0.0001 & -0.0006 & -0.0034 & -0.5332 & 1.0745 & -0.5332 & -0.0033 & -0.0006 & -0.0001 \\ 0. & 0. & -0.0001 & -0.0006 & -0.0034 & -0.5332 & 1.075 & -0.5337 & -0.0034 & -0.0007 \\ 0. & 0. & 0. & -0.0001 & -0.0006 & -0.0033 & -0.5337 & 1.0754 & -0.5338 & -0.004 \\ 0. & 0. & 0. & 0. & -0.0001 & -0.0006 & -0.0034 & -0.5338 & 1.075 & -0.5372 \\ 0. & 0. & 0. & 0. & 0. & -0.0001 & -0.0007 & -0.004 & -0.5372 & 0.5419 \end{bmatrix} \tag{A2}$$

If the conductors in the lower or upper slots are symmetric with the slots, the capacitance matrices of the conductors in the lower and upper slots in (4) will be equal ($\mathbf{C}_{us} = \mathbf{C}_{ls}$). The capacitance matrices of the conductors in the upper slots in nF are:

$$\mathbf{C}_{us} = \begin{bmatrix} 0.6328 & -0.5194 & -0.0002 & 0. & 0. & 0. & 0. & 0. & 0. & 0. \\ -0.5194 & 1.1008 & -0.5198 & -0.0002 & 0. & 0. & 0. & 0. & 0. & 0. \\ -0.0002 & -0.5198 & 1.1012 & -0.5197 & -0.0002 & 0. & 0. & 0. & 0. & 0. \\ 0. & -0.0002 & -0.5197 & 1.1007 & -0.5193 & -0.0002 & 0. & 0. & 0. & 0. \\ 0. & 0. & -0.0002 & -0.5193 & 1.1004 & -0.5193 & -0.0002 & 0. & 0. & 0. \\ 0. & 0. & 0. & -0.0002 & -0.5193 & 1.1004 & -0.5193 & -0.0002 & 0. & 0. \\ 0. & 0. & 0. & 0. & -0.0002 & -0.5193 & 1.1006 & -0.5196 & -0.0002 & 0. \\ 0. & 0. & 0. & 0. & 0. & -0.0002 & -0.5196 & 1.101 & -0.5196 & -0.0002 \\ 0. & 0. & 0. & 0. & 0. & 0. & -0.0002 & -0.5196 & 1.1008 & -0.5194 \\ 0. & 0. & 0. & 0. & 0. & 0. & 0. & -0.0002 & -0.5194 & 0.7054 \end{bmatrix} \tag{A3}$$

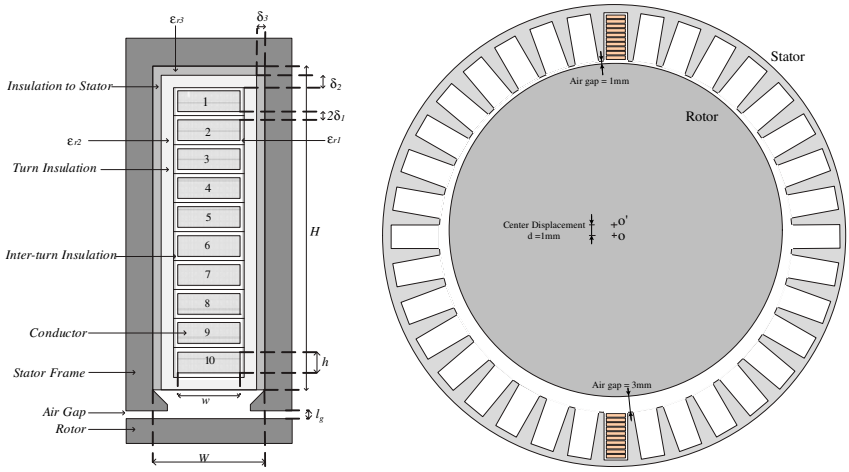

(a) Slot structure (b) Center Displacement

Figure A1. Structure electrical machine.

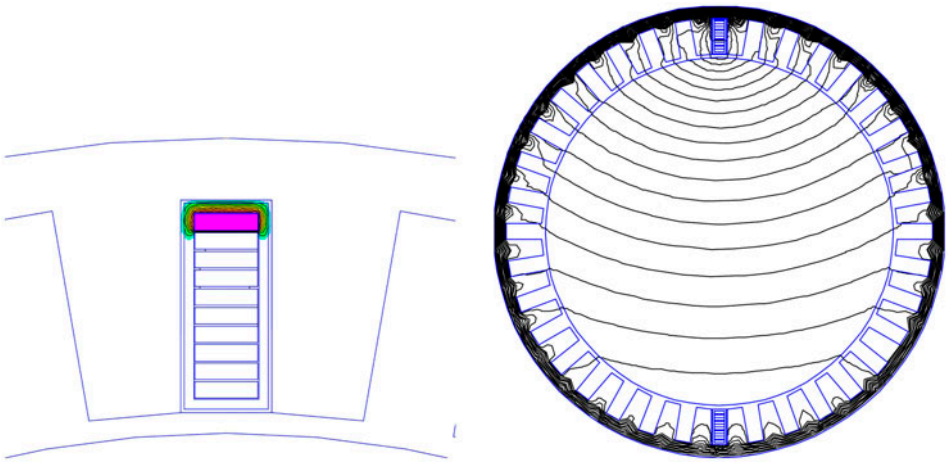

(a) Electric field (b) Magnetic filed

Figure A2. Electric and Magnetic fields in a slot with symmetrical air gap.

Mutual capacitance $\mathbf{C}_m$ and c_r in nF become:

$$\mathbf{C}_m = \begin{bmatrix} -0.0202 & 0. & 0. & 0. & 0. & 0. & 0. & 0. & 0. & 0. & -0.0202 & 0. & 0. & 0. & 0. & 0. & 0. & 0. & 0. & 0 \end{bmatrix}^T$$
$$c_r = 2.1945 \tag{A4}$$

Figure A2(a) shows the electrical field surrounding a conductor captured in the slot but not flowing in the air gap. Thus, the electrical field is not influenced by the air gap and displacement (d) lengths. This illustrates that the capacitance matrices of the conductors are approximately the same in symmetrical and asymmetrical conditions.

Table A1. Comparison of maximum voltage in stator winding with different methods.

Method	$t_s = 400\,\text{ns}$			$l_c = 10\,\text{m}$		
	$l_c = 5\,\text{m}$	$l_c = 10\,\text{m}$	$l_c = 20\,\text{m}$	$t_s = 50\,\text{ns}$	$t_s = 200\,\text{ns}$	$t_s = 600\,\text{ns}$
Proposed model (pu)	1.18	1.37	1.63	1.86	1.80	1.10
Time-domain model (pu) [26]	1.19	1.37	1.63	1.79	1.55	1.15

Table A2. Coaxial cable parameters.

Quantity	Values
Capacitance	600 pf
Inductance	0.3 μ H/m
Resistance (50 Hz)	0.2 mΩ/m
Diameter	20 mm
Conductor diameter	13.7 mm

A.2. Inductance matrix of conductors

The (r, s)th element of the inductance matrix in the kth zone is:

$$L^k_{r,s} = \left.\frac{\Psi^k_r(x,t)}{i^k_s(x,t)}\right|_{\substack{i^k_1(x,t)=\cdots=i^k_{r_k}(x,t)=0 \\ i^k_s(x,t)\neq 0}} \qquad \begin{array}{l} r, s = 1, \cdots, p_k \\ k = FO,\ SR \text{ and } RO \end{array} \tag{A5}$$

in which $\Psi^k_r(x, t)$ is the flux linkage of the rth conductor in the kth zone. The limited factor method is used to calculate the inductance matrix in (3). The sth conductor of the coil in the kth zone is activated by 1 per unit current ($i^k_s(x, t) = 1\ pu$) and the other conductors in this zone are adjusted to zero current. FEM is used to determine the linkage flux for the conductors in the kth zone. Figure A2(c) shows the simulation results using FEM for the proposed machine. Relation (A5) calculates the inductance matrix for a front overhang in μH as:

$$\mathbf{L}_{FO} = \begin{bmatrix} 0.5963 & 0.4567 & 0.3691 & 0.307 & 0.2599 & 0.2226 & 0.1922 & 0.1669 & 0.1453 & 0.1267 \\ 0.4567 & 0.6022 & 0.4619 & 0.3735 & 0.3106 & 0.2629 & 0.2251 & 0.1942 & 0.1683 & 0.1462 \\ 0.3691 & 0.4619 & 0.6066 & 0.4656 & 0.3765 & 0.313 & 0.2648 & 0.2265 & 0.1951 & 0.1688 \\ 0.307 & 0.3735 & 0.4656 & 0.6096 & 0.4681 & 0.3784 & 0.3144 & 0.2657 & 0.227 & 0.1951 \\ 0.2599 & 0.3106 & 0.3765 & 0.4681 & 0.6115 & 0.4695 & 0.3792 & 0.3148 & 0.2657 & 0.2265 \\ 0.2226 & 0.2629 & 0.313 & 0.3784 & 0.4695 & 0.6124 & 0.4697 & 0.3791 & 0.3142 & 0.2646 \\ 0.1922 & 0.2251 & 0.2648 & 0.3144 & 0.3792 & 0.4697 & 0.6122 & 0.4691 & 0.378 & 0.3126 \\ 0.1669 & 0.1942 & 0.2265 & 0.2657 & 0.3148 & 0.3791 & 0.4691 & 0.6109 & 0.4674 & 0.3758 \\ 0.1453 & 0.1683 & 0.1951 & 0.227 & 0.2657 & 0.3142 & 0.378 & 0.4674 & 0.6086 & 0.4645 \\ 0.1267 & 0.1462 & 0.1688 & 0.1951 & 0.2265 & 0.2646 & 0.3126 & 0.3758 & 0.4645 & 0.6051 \end{bmatrix} \tag{A6}$$

The inductance matrices of the front and rear overhangs are equal ($\mathbf{L}_{FO} = \mathbf{L}_{RO}$) for the symmetrical structure of the winding in the proposed machine. Moreover, if the conductors in the upper and lower slots are symmetric ($d = 0$), the inductance matrices for these conductors will be equal ($\mathbf{L}_{us} = \mathbf{L}_{ls}$). The inductance matrix in μH becomes:

Table A3. Main parameters of stator winding.

Quantity	Symbol	Values
Slot width	W	8.9 mm
Slot length	l	0.38 m
Slot height	H	20.07 mm
Air gap length	l_g	2 mm
Overhang length	$l_3,\ l_4$	0.2 m
Conductors width	w	6.08 mm
Conductors height	h	1.59 mm
Resistivity of stator bar conductors	ρ_b	$1.7 \times 10^{-8}\ \Omega$m
Conductances of stator bar conductors	g_p	neglected
Thickness of inter-turn insulation	δ_1	0.11 mm
Thickness of turn insulation	δ_2	0.96 mm
Thickness of insulation to stator	δ_3	0.33 mm
Relative permittivity of inter-turn insulation	ϵ_{r1}	2.5
Relative permittivity of turn insulation	ϵ_{r2}	2
Relative permittivity of insulation to stator	ϵ_{r3}	4

$$\mathbf{L}_{us}|_{d=0} = \begin{bmatrix} 43.3835 & 43.3856 & 43.3632 & 43.348 & 43.3348 & 43.3223 & 43.3103 & 43.2987 & 43.2877 & 43.2776 \\ 43.3856 & 43.5953 & 43.6046 & 43.5838 & 43.5691 & 43.5562 & 43.544 & 43.5322 & 43.5211 & 43.511 \\ 43.3632 & 43.6046 & 43.8208 & 43.8316 & 43.8114 & 43.797 & 43.7843 & 43.7723 & 43.7611 & 43.7509 \\ 43.348 & 43.5838 & 43.8316 & 44.0498 & 44.0609 & 44.0411 & 44.0268 & 44.0144 & 44.003 & 43.9927 \\ 43.3348 & 43.5691 & 43.8114 & 44.0609 & 44.2797 & 44.2911 & 44.2715 & 44.2576 & 44.2457 & 44.2352 \\ 43.3223 & 43.5562 & 43.797 & 44.0411 & 44.2911 & 44.51 & 44.5218 & 44.5025 & 44.4892 & 44.4782 \\ 43.3103 & 43.544 & 43.7843 & 44.0268 & 44.2715 & 44.5218 & 44.741 & 44.7531 & 44.7344 & 44.722 \\ 43.2987 & 43.5322 & 43.7723 & 44.0144 & 44.2576 & 44.5025 & 44.7531 & 44.9727 & 44.9854 & 44.9676 \\ 43.2877 & 43.5211 & 43.7611 & 44.003 & 44.2457 & 44.4892 & 44.7344 & 44.9854 & 45.2054 & 45.2195 \\ 43.2776 & 43.511 & 43.7509 & 43.9927 & 44.2352 & 44.4782 & 44.722 & 44.9676 & 45.2195 & 45.4419 \end{bmatrix} \tag{A7}$$

Similarly, the inductance matrix of the upper conductors in an asymmetrical condition ($d = 1$) can be determined as:

$$\mathbf{L}_{us}|_{d=1} = \begin{bmatrix} 50.8074 & 50.8025 & 50.7762 & 50.758 & 50.7422 & 50.7274 & 50.713 & 50.6992 & 50.6862 & 50.6743 \\ 50.8025 & 51.0053 & 51.0105 & 50.9869 & 50.9696 & 50.9543 & 50.9397 & 50.9258 & 50.9127 & 50.9007 \\ 50.7762 & 51.0105 & 51.223 & 51.2308 & 51.2081 & 51.1912 & 51.1762 & 51.1621 & 51.1489 & 51.1368 \\ 50.758 & 50.9869 & 51.2308 & 51.4459 & 51.4557 & 51.4324 & 51.4159 & 51.4013 & 51.3879 & 51.3757 \\ 50.7422 & 50.9696 & 51.2081 & 51.4547 & 51.6708 & 51.6799 & 51.6579 & 51.6419 & 51.628 & 51.6157 \\ 507274 & 50.9543 & 51.1912 & 51.4324 & 51.6799 & 518963 & 51.9059 & 51.8844 & 51.869 & 51.8562 \\ 50.713 & 50.9397 & 51.1762 & 51.4159 & 51.6579 & 51.9059 & 52.1227 & 52.1327 & 52.1119 & 52.0977 \\ 50.6992 & 50.9258 & 51.1621 & 51.4013 & 51.6419 & 51.8844 & 52.1327 & 52.3501 & 52.3608 & 52.3412 \\ 50.6862 & 50.9127 & 51.1489 & 51.3879 & 51.628 & 51.869 & 52.1119 & 52.3608 & 52.5788 & 52.591 \\ 50.6743 & 50.9007 & 51.1368 & 51.3757 & 51.6157 & 51.8562 & 52.0977 & 52.3412 & 52.591 & 52.8116 \end{bmatrix} \tag{A8}$$

Results in (A7) and (A8) show that displacement distance had a noticeable effect upon the inductance matrices. The coupling inductance matrices do not depend on d. The matrices of the coupling inductances in the symmetrical and asymmetrical cases are similar as:

Table A4. Front & rear bearing parameters.

Quantity	Symbol	Values
Capacitance	$C_{fb} = C_{rb}$	5 pf
Series resistance	$R_{fb} = R_{rb}$	0.65 mΩ
Capacitor conductance	$G_{fb} = G_{rb}$	10^{-3} ℧
Conductance	$G'_{fb} = G'_{rb}$	neglected

$$\mathbf{L}_{uls} = \begin{bmatrix} 15.4339 & 15.4299 & 15.4257 & 15.4216 & 15.4174 & 15.4133 & 15.4093 & 15.4053 & 15.4015 & 15.398 \\ 15.4299 & 15.4258 & 15.4217 & 15.4176 & 15.4134 & 15.4093 & 15.4052 & 15.4013 & 15.3975 & 15.394 \\ 15.4257 & 15.4217 & 15.4176 & 15.4134 & 15.4093 & 15.4052 & 15.4011 & 15.3972 & 15.3934 & 15.3899 \\ 15.4216 & 15.4176 & 15.4134 & 15.4093 & 15.4051 & 15.401 & 15.397 & 15.393 & 15.3892 & 15.3857 \\ 15.4174 & 15.4134 & 15.4093 & 15.4051 & 15.401 & 15.3969 & 15.3928 & 15.3889 & 15.3851 & 15.3816 \\ 15.4133 & 15.4093 & 15.4052 & 15.401 & 15.3969 & 15.3928 & 15.3887 & 15.3848 & 15.381 & 15.3775 \\ 15.4093 & 15.4052 & 15.4011 & 15.397 & 15.3928 & 15.3887 & 15.3847 & 15.3807 & 15.3769 & 15.3734 \\ 15.4053 & 15.4013 & 15.3971 & 15.393 & 15.3889 & 15.3848 & 15.3807 & 15.3767 & 15.3729 & 15.3695 \\ 15.4015 & 15.3975 & 15.3933 & 15.3892 & 15.3851 & 15.381 & 15.3769 & 15.3729 & 15.3692 & 15.3657 \\ 15.398 & 15.394 & 15.3898 & 15.3857 & 15.3816 & 15.3774 & 15.3734 & 15.3694 & 15.3657 & 15.3622 \end{bmatrix} \tag{A9}$$

$$\mathbf{L}_m = [\ 23.8827 \quad 23.8763 \quad 23.8699 \quad 23.8634 \quad 23.857 \quad 23.8506 \quad 23.8443 \quad 23.8381 \quad 23.8322 \quad 23.8268$$
$$23.8441, 23.8377, 23.8313, 23.8248, 23.8184, 23.812, 23.8058, 23.7996, 23.7937, 23.7883]^T$$
$$L_r = 123.492 \tag{A10}$$